PP2A-B56 opposes Mps1 phosphorylation of Knl1 and thereby promotes spindle assembly checkpoint silencing

Antonio Espert,[1] Pelin Uluocak,[1] Ricardo Nunes Bastos,[2] Davinderpreet Mangat,[1] Philipp Graab,[1] and Ulrike Gruneberg[1]

[1]Sir William Dunn School of Pathology and [2]Department of Biochemistry, University of Oxford, Oxford OX1 3RE, England, UK

The spindle assembly checkpoint (SAC) monitors correct attachment of chromosomes to microtubules, an important safeguard mechanism ensuring faithful chromosome segregation in eukaryotic cells. How the SAC signal is turned off once all the chromosomes have successfully attached to the spindle remains an unresolved question. Mps1 phosphorylation of Knl1 results in recruitment of the SAC proteins Bub1, Bub3, and BubR1 to the kinetochore and production of the wait-anaphase signal. SAC silencing is therefore expected to involve a phosphatase opposing Mps1. Here we demonstrate in vivo and in vitro that BubR1-associated PP2A-B56 is a key phosphatase for the removal of the Mps1-mediated Knl1 phosphorylations necessary for Bub1/BubR1 recruitment in mammalian cells. SAC silencing is thus promoted by a negative feedback loop involving the Mps1-dependent recruitment of a phosphatase opposing Mps1. Our findings extend the previously reported role for BubR1-associated PP2A-B56 in opposing Aurora B and suggest that BubR1-bound PP2A-B56 integrates kinetochore surveillance and silencing of the SAC.

Introduction

Mps1-dependent spindle assembly checkpoint (SAC) signaling delays anaphase entry until all chromosomes have been correctly attached to the mitotic spindle (Foley and Kapoor, 2013). Knl1 is the kinetochore localized binding partner for the SAC proteins Bub1, BubR1, and Bub3 (Kiyomitsu et al., 2007). Phosphorylation of Knl1 by Mps1 is a prerequisite for the interaction of Bub1 and Bub3 with Knl1 (Schittenhelm et al., 2009; Krenn et al., 2012, 2014; London et al., 2012; Shepperd et al., 2012; Yamagishi et al., 2012; Primorac et al., 2013; Vleugel et al., 2013). Once amphitelic kinetochore attachment has been achieved, the kinetochore levels of Bub1, Bub3, and BubR1 drop (Funabiki and Wynne, 2013). This SAC silencing process requires the reversal of Mps1-mediated phosphorylations on Knl1 to stop further recruitment of SAC proteins and production of the wait-anaphase signal. In yeast, PP1 is an important SAC phosphatase promoting SAC silencing by opposing Mps1, as well as Aurora B (Pinsky et al., 2009; Vanoosthuyse and Hardwick, 2009; Meadows et al., 2011; Rosenberg et al., 2011; London et al., 2012). While in mammalian cells a BubR1-associated pool of PP2A-B56 has recently been shown to oppose Aurora B (Foley et al., 2011; Suijkerbuijk et al., 2012; Kruse et al., 2013; Xu et al., 2013), the phosphatase opposing Mps1 has not been identified. Here we use an unbiased screen for SAC phosphatase activity to demonstrate that BubR1-associated PP2A-B56 is a key phosphatase for the removal of the Mps1-mediated Knl1 phosphorylations necessary for Bub1/BubR1 recruitment. We suggest that SAC silencing is promoted by a negative feedback loop formed by Mps1-dependent recruitment of a phosphatase that opposes its own action.

A. Espert and P. Uluocak contributed equally to this paper.

Correspondence to Ulrike Gruneberg: ulrike.gruneberg@path.ox.ac.uk

P. Graab's present address is Institute of Biochemistry, Biocenter Goethe-Universität Frankfurt, 60438 Frankfurt/Main, Germany.

Abbreviations used in this paper: PPP, phosphoprotein phosphatase; SAC, spindle assembly checkpoint.

Supplemental material can be found at:
http://doi.org/10.1083/jcb.201406109

The Rockefeller University Press $30.00
J. Cell Biol. Vol. 206 No. 7 833–842
www.jcb.org/cgi/doi/10.1083/jcb.201406109

Results and discussion

PP2A opposes Mps1-dependent kinetochore localization of BubR1 and Bub1

To investigate the role of dephosphorylation in the early events of SAC silencing (Fig. 1 A), we developed an assay in which SAC arrested cells are treated with a brief pulse of the specific Mps1 inhibitor AZ3146 to synchronously inactivate the checkpoint (Hewitt et al., 2010). Downstream events and mitotic exit are prevented by simultaneous addition of the proteasome inhibitor MG132. In control cells, Mps1 inhibition resulted in the loss of BubR1 and Bub1 from the kinetochore within 5 min (Fig. S1 A), which confirms the dependence of these SAC proteins on Mps1 activity for localization (Maciejowski et al., 2010; Sliedrecht et al., 2010). Mps1 inhibition in the presence of the general phosphoprotein phosphatase (PPP) inhibitor calyculin A resulted in retention of BubR1 and Bub1 at kinetochores (Fig. 1, B and C). Since Bub1 behaved identically to BubR1 in all experiments, BubR1 staining is representative of both Bub1 and BubR1 in all figures. Our observations indicate the presence of a highly active PPP-family phosphatase in SAC-arrested cells, promoting rapid dissociation of Bub1 and BubR1 from kinetochores in the absence of opposing Mps1 activity (see the model in Fig. 1 A).

To identify the specific PPP phosphatase, SAC inactivation assays were performed in cells depleted of the PPP family catalytic subunits, PP1–6 (Fig. 1 D). Under these conditions, BubR1 levels at the kinetochore remained similar to the control (Fig. 1 D, Mps1 active/Control), which indicates that the SAC was still active. Although all PPP-family catalytic subunits were efficiently depleted (Fig. 1 F), only depletion of the PP2A catalytic subunit α, or α and β together, resulted in quantitative retention of the BubR1 signal (Fig. 1 D, Mps1 inactive/Mps1 inhibition; and Fig. 1 E). Because Knl1-associated PP1 had previously been identified as the phosphatase opposing Knl1 phosphorylation by Mps1 in yeast (London et al., 2012), and PP1α and PP1γ had also been shown to interact with human Knl1 (Liu et al., 2010), we further investigated the potential involvement of PP1α and PP1γ. To test for potential redundancy between these two PP1 catalytic subunits, PP1α and -γ were depleted together and for longer (84 h). Under these conditions, haspin-dependent histone H3 phospho Thr3 staining, a known PP1 target (Qian et al., 2011), was efficiently retained in the presence of the haspin inhibitor 5-iodotubercidine (De Antoni et al., 2012), confirming functional knockdown of PP1α and -γ (Fig. S1 B). Nevertheless, protection of BubR1 kinetochore localization upon Mps1 inhibition was not observed (Fig. S1 C). Therefore, under these conditions a PP2A phosphatase opposes Mps1 activity in SAC-arrested human cells, whereas PP1 does not. We thus focused on PP2A as a candidate phosphatase initiating Knl1 dephosphorylation during SAC silencing.

A PP2A-B56 holoenzyme complex regulates Bub1 and BubR1 kinetochore localization

PP2A holoenzymes consist of a catalytic subunit, a scaffolding subunit (PP2A-A), and a member of one of four families of regulatory subunits B, B′, B″, or B‴. The B (PP2A-B55) and B′ (PP2A-B56) families are most relevant for mitotic progression in mammalian cells (Bollen et al., 2009; Barr et al., 2011). To define the PP2A holoenzyme complex promoting release of BubR1/Bub1 from the kinetochore, cells were depleted of the PP2A scaffolding subunit, PP2A-A, or all subunits of the PP2A-B55 and -B56 regulatory subunit families (Foley et al., 2011; Cundell et al., 2013; Fig. 2, A and B). Western blotting of selected PP2A-B55 or -B56 subunits demonstrated efficient depletion (Fig. 2 C). Removal of the main PP2A scaffolding subunit PP2A-A as well as depletion of all B56, but not B55 subunits, resulted in the retention of BubR1 kinetochore signal (Fig. 2, A and B). Furthermore, live cell imaging of PP2A-B56–depleted HeLa cells expressing GFP-BubR1 showed a strongly delayed loss of kinetochore GFP signal upon Mps1 inhibition (Fig. 2, D and E). Further investigation revealed that although full retention of BubR1 kinetochore localization was only achieved when all B56 subunits were depleted simultaneously, PP2A-B56δ was the largest single contributor to this activity (Fig. S2, A–C). Together, these results show that the PP2A holoenzyme regulating BubR1 and Bub1 kinetochore association consists of PP2ACα/β, PP2A-A, and PP2A-B56 (Fig. 2, A and B), and point to a potential redundancy between PP2A-B56 isoforms, also observed in other studies (Foley et al., 2011; Suijkerbuijk et al., 2012; Kruse et al., 2013; Xu et al., 2013).

Delayed mitotic exit in the absence of PP2A-B56

PP2A-B56 has recently been found to regulate microtubule–kinetochore attachments by opposing Aurora B and Plk1 activity, resulting in severe chromosome alignment problems in the absence of PP2A-B56 (Foley et al., 2011). Live-cell imaging of GFP-tubulin histone H2B-mCherry HeLa cells revealed a persistent prometaphase arrest when cells were depleted of all PP2A-B56 subunits (Fig. S2 D). Our data suggest that this arrest is caused by a combination of the inability to initiate SAC silencing by dephosphorylating Knl1, and persistent SAC activation caused by incorrect microtubule–kinetochore attachments (Foley et al., 2011; Suijkerbuijk et al., 2012; Kruse et al., 2013; Xu et al., 2013). To separate the role of PP2A-B56 in SAC silencing from its role in promoting microtubule–kinetochore attachment, mitotic PP2A-B56–depleted cells were treated with the Mps1 inhibitor AZ3146 to overcome the persistent SAC activation and induce mitotic exit. In this situation, PP2A-B56–depleted mitotic cells required significantly more time to initiate sister chromatid separation than control cells (on average, 27.75 ± 4.74 min in siPP2A-B56 cells [$n = 12$] versus 7.27 ± 1.74 min in control cells [$n = 10$]; Fig. 2, F and G). This strongly suggests a requirement for PP2A-B56 in the silencing of the SAC in addition to its known role in stabilizing microtubule–kinetochore interactions.

PP2A-B56 dephosphorylates Mps1-phosphorylated Knl1

Bub1 and BubR1 binding to the kinetochore is dependent on Mps1-phosphorylated Knl1 (London et al., 2012; Shepperd et al.,

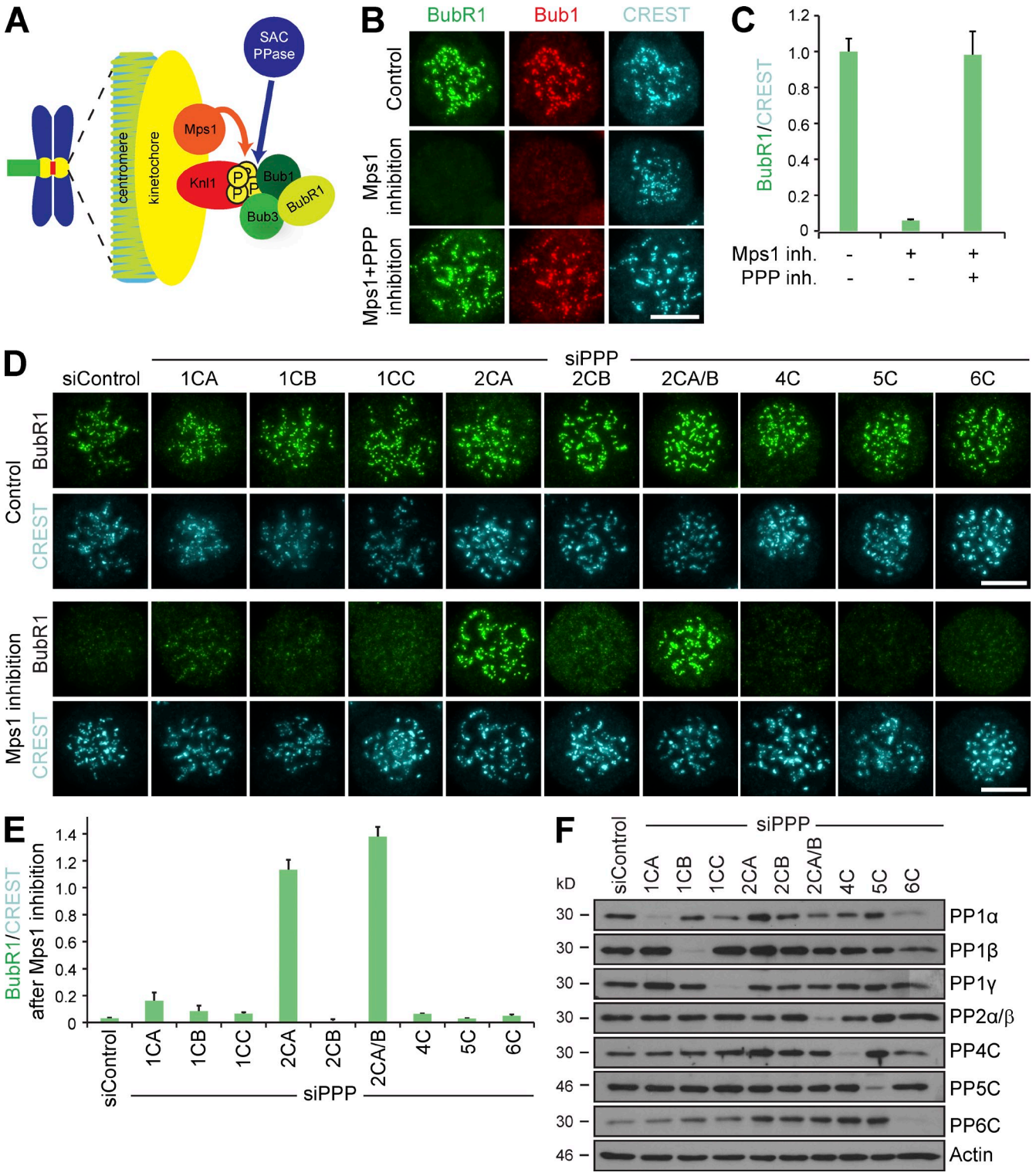

Figure 1. **BubR1 and Bub1 localization to kinetochores is negatively regulated by PP2A.** (A) Mps1 phosphorylation of Knl1 recruits Bub1, Bub3, and BubR1. An unidentified SAC phosphatase opposes Mps1 and controls kinetochore release of Bub proteins. (B) Nocodazole-arrested HeLa cells were treated with MG132 (control), an MG132/Mps1 inhibitor AZ3146 mix (Mps1 inhibition), or preincubated for 3 min with 25 nM calyculin A before AZ3146/MG132 addition (Mps1 + PPP inhibition). Cells were fixed and stained for Bub1, BubR1, and kinetochores (CREST). Bar, 10 µm. (C) CREST-normalized BubR1 kinetochore intensity was plotted (mean ± SD [error bars]; $n \geq 120$ kinetochores per bar). (D) HeLa cells depleted of individual PPP family catalytic subunits were nocodazole arrested, treated for 5 min with either MG132 or MG132/AZ3146, fixed, and stained for BubR1 and kinetochores (CREST). Bar, 10 µm. (E) Quantitation of the ratio of CREST-normalized BubR1 signal in control and AZ3146-treated cells (mean ± SD [error bars]; $n \geq 120$ kinetochores per bar). Images shown are representative of three independent experiments. (F) Cell lysates of the cells used in D were blotted as indicated.

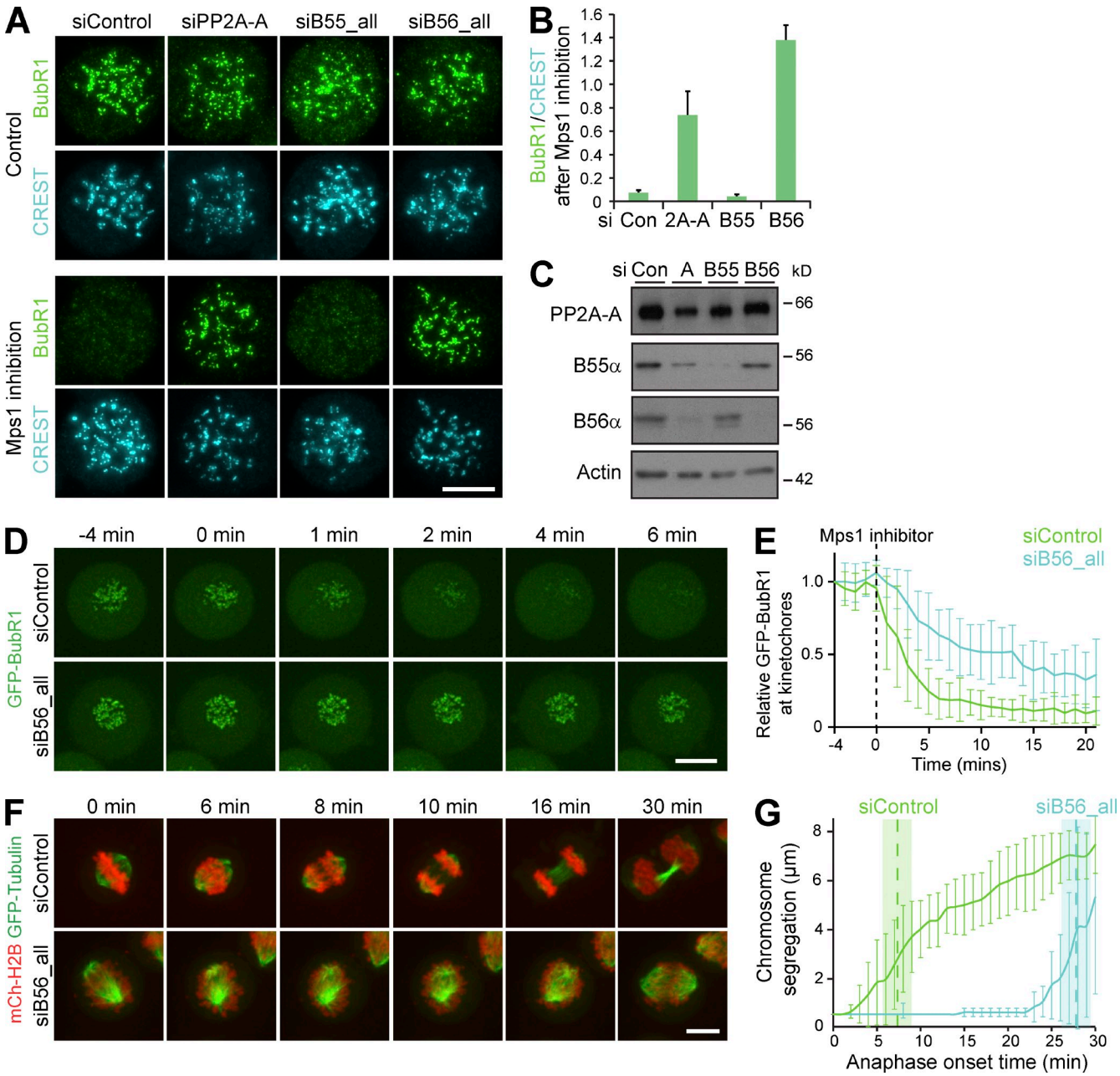

Figure 2. **PP2A-B56 opposes Mps1 in targeting BubR1 to the kinetochore.** (A) HeLa cells were depleted of PP2A-A, all PP2A-B55, or all PP2A-B56 subunits, arrested with nocodazole, and then treated and stained as in Fig. 1 D. (B) The ratio of CREST-normalized BubR1 signal in control and AZ3146-treated cells was plotted (mean ± SD; $n \geq 120$ kinetochores per bar). Images are representative of three independent experiments. (C) Lysates of the cells used in A were blotted as indicated. Note that depletion of PP2A-A leads to reduced levels of B55α and B56α due to impaired holoenzyme complex formation. (D) Control or PP2A-B56–depleted nocodazole-arrested GFP-BubR1 HeLa Flp-in cells were imaged for 4 min and then treated with AZ3146. Image stacks were taken every minute. Representative maximum projections are shown. (E) GFP-BubR1 kinetochore signals were plotted against time ($n = 12$ for control, $n = 9$ for siB56_all; mean ± SD [error bars]). (F) GFP–α-tubulin/mCherry-histone H2B HeLa cells were treated with AZ3146 at the meta/pseudometaphase stage (t = 0). Image stacks were taken every minute. Representative maximum projections are shown; $n = 10$ for control, $n = 12$ for siB56_all. (G) The distance between the retreating chromatin masses was plotted against time (mean ± SD [error bars]). Anaphase entry (broken line indicates the mean) was defined as the first frame with visibly segregated sister chromatids. Bars, 10 μm.

2012; Yamagishi et al., 2012). To demonstrate that PP2A-B56 dephosphorylates this form of Knl1, an antibody was raised against one of the conserved Mps1 phosphorylation sites on Knl1, pT875 (Yamagishi et al., 2012). Staining with anti–pKnl1-pT875 was dependent on the presence of Knl1 and Mps1 activity (Fig. S3, A and B). Importantly, the loss of pKnl1-pT875 signal upon Mps1 inhibitor treatment could be prevented by depleting all PP2A-B56 but not PP2A-B55 regulatory subunits (Fig. 3, A and B). This suggested that PP2A-B56 dephosphorylates pKnl1-pT875. Consistent with this idea, we observed an almost twofold increase in pKnl1-pT875 signal in asynchronously cycling cells depleted of PP2A-B56 (Fig. 3, C and D).

To verify that Knl1 is a direct PP2A-B56 substrate, GST-tagged Knl1$^{728\text{-}1200}$ or Knl1$^{728\text{-}1200\text{-}T875A}$, in which the

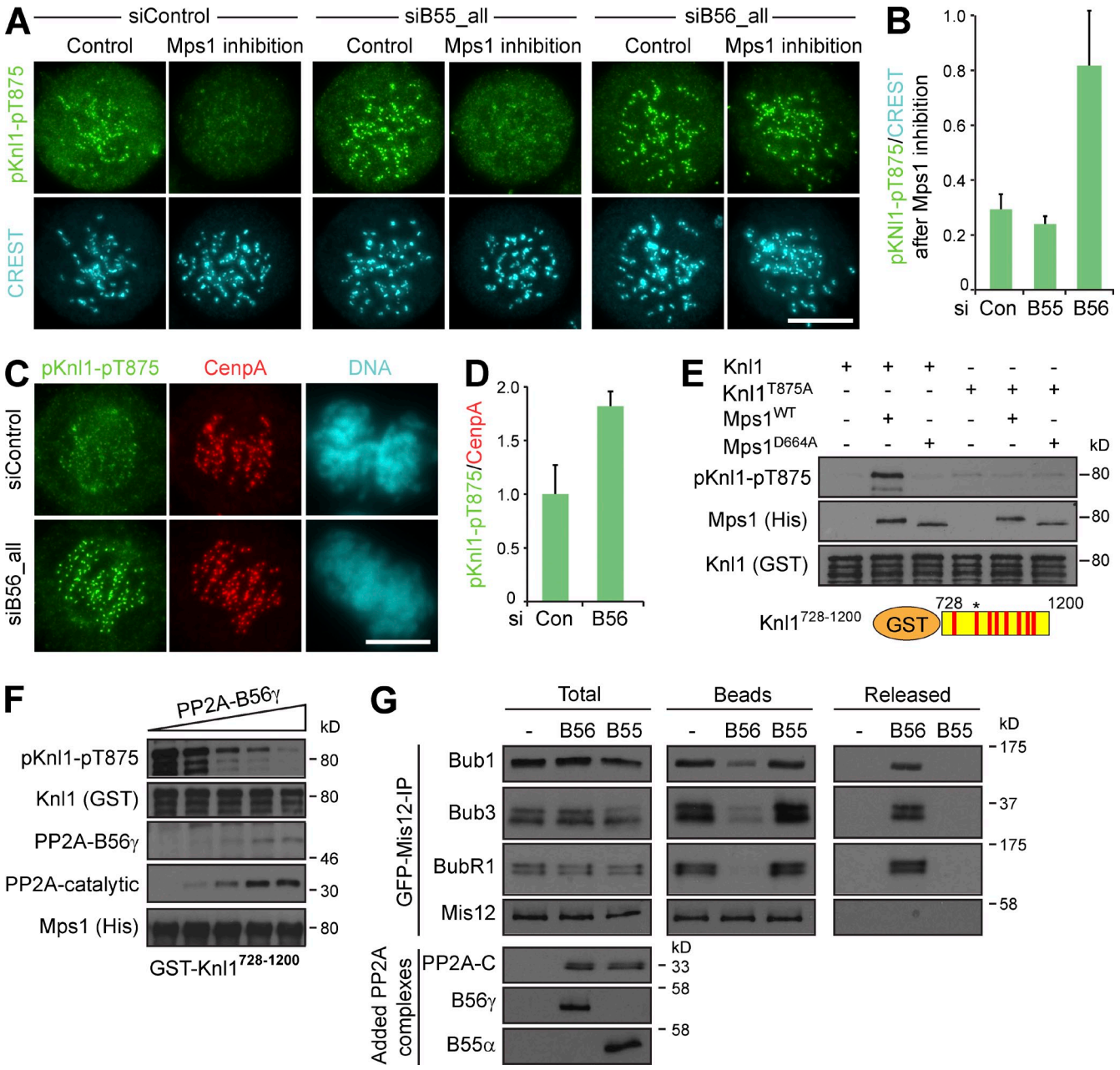

Figure 3. **PP2A-B56 is a Knl1 phosphatase.** (A) Nocodazole-arrested HeLa cells depleted of all PP2A-B55 subunits or all PP2A-B56 subunits were treated with MG132 or MG132/AZ3146 for 5 min, fixed, and stained for pKnl1-pT875 and kinetochores (CREST). Bar, 10 µm. Images are representative of three independent experiments. (B) The ratio of CREST-normalized pKnl1-pT875 signal in control and AZ3146-treated cells was plotted (mean ± SD [error bars]; $n \geq 120$ kinetochores per bar). (C) Asynchronously cycling cells were fixed and stained for pKnl1-pT875, CenpA, and DNA (DAPI). Bar, 10 µm. (D) Quantitation of the CenpA-normalized pKnl1-pT875 signal in control and PP2A-B56–depleted cells (mean ± SD; $n \geq 120$ kinetochores per bar). (E) GST-Knl1$^{728\text{-}1200}$ or GST-Knl1$^{728\text{-}1200\text{-}T875A}$ was phosphorylated with Mps1^{WT} or kinase-dead Mps1^{D664A}. T875-phosphorylated GST-Knl1$^{728\text{-}1200}$ was detected by Western blotting using the pKnl1-pT875 antibody. Equal loading of Knl1 substrate and the addition of equivalent amounts of Mps1^{WT} and Mps1^{D664A} was confirmed by Western blotting. The asterisk indicates the position of the phosphorylated threonine recognized by the pKnl1-pT875 antibody. (F) GST-Knl1$^{728\text{-}1200}$ was phosphorylated with Mps1^{WT}, Mps1 was inhibited by the addition of AZ3146, and phospho-Knl1 was dephosphorylated by the addition of PP2A-B56 (Cundell et al., 2013). The final amounts of PP2A complexes in the different lanes of the assay were 0, 3.6, 8.75, 17.5, and 27 nM. pKnl1-pT875 and PP2A-B56 were visualized by Western blotting. Equal loading of GST-Knl1$^{728\text{-}1200}$ and Mps1 was confirmed by Western blotting with anti-GST (Knl1) and anti-His (Mps1) antibodies. (G) GFP-Mis12 complexes with associated Knl1 and SAC proteins were purified from GFP-Mis12 HeLa cells. The immunoprecipitates were incubated with PP2A-B55 or PP2A-B56 and analyzed by Western blotting.

phospho-acceptor threonine 875 had been mutated to alanine, was in vitro phosphorylated by Mps1^{WT} or catalytically inactive Mps1^{D664A}. The phosphorylated protein was then detected by pKnl1-pT875 antibodies (Fig. 3 E). Confirming published reports, GST-Knl1$^{728\text{-}1200}$ was readily phosphorylated by Mps1^{WT} but not Mps1^{D664A} (London et al., 2012; Shepperd et al., 2012; Yamagishi et al., 2012; Fig. 3 E). GST-Knl1$^{728\text{-}1200\text{-}T875A}$ was not detected by antibodies against pKnl1-pT875 after incubation with Mps1^{WT}, confirming the specificity of our antibody (Fig. 3 E). Mps1-phosphorylated GST-Knl1$^{728\text{-}1200}$ was then incubated

with purified PP2A-B56γ complexes (Cundell et al., 2013; Fig. 3 F). Titration of this PP2A enzyme complex demonstrated effective dephosphorylation of phosphorylated GST-Knl1$^{728\text{-}1200}$ by 27 nM PP2A-B56γ, comparable to the amount of PP2A-B55 required to achieve tau dephosphorylation (20 nM; Xu et al., 2008; Fig. 3 F). To test dephosphorylation of phospho-Knl1 by PP2A complexes in a more physiological setting, GFP-Mis12 immunoprecipitates with associated Knl1 and SAC proteins (Kiyomitsu et al., 2007; Welburn et al., 2010) were incubated with equivalent amounts of PP2A-B56 and PP2A-B55, and supernatant and beads were separated and analyzed (Fig. 3 G). Addition of PP2A-B56 but not PP2A-B55 released Mis12 complex associated Bub1, Bub3, and BubR1 into the supernatant and reduced the pKNl1-pT875 signal on the beads, which is consistent with dephosphorylation of phospho-Knl1 by PP2A-B56 but not PP2A-B55 (Fig. 3 G and Fig. S3 C).

BubR1-bound PP2A-B56 regulates kinetochore release of BubR1 and Bub1

Our data so far indicate that PP2A-B56 is a key phosphatase for the dephosphorylation of Mps1-phosphorylated Knl1. Loss of localized PP2A-B56 activity should thus lead to retention of Bub1 and BubR1 at the kinetochore in the absence of Mps1 activity. Recent studies indicate that two pathways exist to localize PP2A-B56 to the centromere and kinetochore region of mammalian chromosomes. First, PP2A-B56 is targeted to the centromere by interaction with Sgo2, one of the two shugoshin proteins in mammalian cells (Kitajima et al., 2006; Xu et al., 2009; Tanno et al., 2010), and second, a distinct pool of PP2A-B56 is localized to the outer kinetochore via the SAC protein BubR1 (Suijkerbuijk et al., 2012; Kruse et al., 2013; Xu et al., 2013). Although Sgo2 depletion resulted in a strong reduction of centromeric PP2A-B56α (Fig. S3, D and E; Tanno et al., 2010), loss of kinetochore BubR1 upon Mps1 inhibition was not affected (Fig. S3F), which indicates that Sgo2-bound PP2A-B56 does not contribute to phospho-Knl1 dephosphorylation. In contrast, replacement of endogenous BubR1 with equivalent, physiological levels of GFP-BubR1^{WT} or GFP-BubR1$^{L669A/I672A}$, mutant for PP2A-B56 binding (Kruse et al., 2013), demonstrated that cells expressing GFP-BubR1$^{L669A/I672A}$, but not GFP-BubR1^{WT}, retained both GFP-BubR1 and endogenous Bub1 on the kinetochore after Mps1 inhibition (Fig. 4, A–C). Furthermore, when progressing through an undisturbed cell cycle, cells expressing only GFP-BubR1$^{L669A/I672A}$ retained high GFP-BubR1 levels on kinetochores and remained on average three times longer in mitosis than GFP-BubR1^{WT} cells (Fig. 4, D–F). Confirming this, in fixed GFP-BubR1^{WT} cells approximately half of all mitotic figures were in anaphase after 11 h of release from a thymidine block, as indicated by separated DNA masses and loss of securin staining (Fig. 4 G). In contrast, cells expressing GFP-BubR1$^{L669A/I672A}$ displayed a markedly higher proportion of prometaphase figures and almost no anaphase figures (Fig. 4 G), which indicates that the absence of BubR1-associated PP2A-B56 delayed mitotic exit due to a combined effect of impaired microtubule–kinetochore attachment formation (Suijkerbuijk et al., 2012; Kruse et al., 2013; Xu et al., 2013) and an inability to release Bub1 and BubR1 from the kinetochores and silence the SAC (Fig. 4, D and G). Together, these findings suggest that BubR1-associated PP2A-B56 establishes a negative feedback loop affecting its own recruitment (Fig. 4 H) and regulating SAC silencing and anaphase entry.

Regulation of the SAC by PP2A-B56

We have shown that in mammalian cells, a key phosphatase for the dephosphorylation of the Bub1/Bub3/BubR1 phospho-binding sites on Knl1 is BubR1-associated PP2A-B56 (see Fig. 5 for model). This result is intriguing because in yeast, Knl1-associated PP1 has been shown to be the phosphatase responsible for reversing the Mps1-mediated phosphorylation of Knl1/spc105/Spc7, and Knl1-bound PP1 had also been implicated in SAC silencing in metazoan cells (Espeut et al., 2012; London et al., 2012; Zhang et al., 2014). Although these studies undisputedly indicate a requirement for PP1 in SAC silencing, it has also been demonstrated that in mammalian cells PP1γ can only associate with Knl1 once the Aurora B–phosphorylated PP1-binding SILK and RVSF motifs in the N terminus of Knl1 have been dephosphorylated upon microtubule–kinetochore attachment and physical separation of centromeric Aurora B and kinetochore-localized Knl1 (Liu et al., 2010). Thus, in SAC-arrested cells, as used in our experiments, or directly after microtubule binding, PP1γ would not be bound to the kinetochore (Liu et al., 2010) and not be available for initial Knl1 dephosphorylation. An interesting possibility is that PP2A-B56 dephosphorylates both the Mps1 and Aurora B sites on Knl1 and thus switches Knl1 from a SAC-ON to a SAC-OFF state. PP1 may then take over from PP2A-B56 to completely dephosphorylate mitotically phosphorylated kinetochore proteins including Knl1 itself.

PP2A-B56 complexes exist in different pools in mammalian mitotic cells. Centromeric Sgo1- and Sgo2-associated PP2A-B56 mediates the protection of centromeric cohesion (Kitajima et al., 2006; Xu et al., 2009; Tanno et al., 2010), whereas a kinetochore, BubR1-associated pool of PP2A-B56 regulates chromosome alignment by opposing Aurora B activity (Foley et al., 2011; Suijkerbuijk et al., 2012; Kruse et al., 2013; Xu et al., 2013). The data presented here indicate that the same pool of PP2A-B56 also regulates SAC silencing by dephosphorylating the Knl1 binding surface for Bub1/Bub3/BubR1. BubR1-bound PP2A-B56 is thus responsible for the initial removal of the Bub proteins from the kinetochores upon loss of Mps1 activity, either by experimental Mps1 inhibition as used here (Fig. 1 B) or by physiological rapid Mps1 displacement from the kinetochore upon SAC satisfaction (Jelluma et al., 2010). It is intriguing that PP2A-B56 controls both the formation of stable microtubule–kinetochore attachments by opposing Aurora B and the initiation of SAC silencing by opposing Mps1, and suggests that this phosphatase has a key role in integrating the two events.

Association of PP2A-B56 with BubR1 creates a situation where BubR1 recruits the factor that drives its own release from the kinetochore, creating a negative feedback loop (Figs. 4 H and 5). This constellation has two clear advantages. First, a

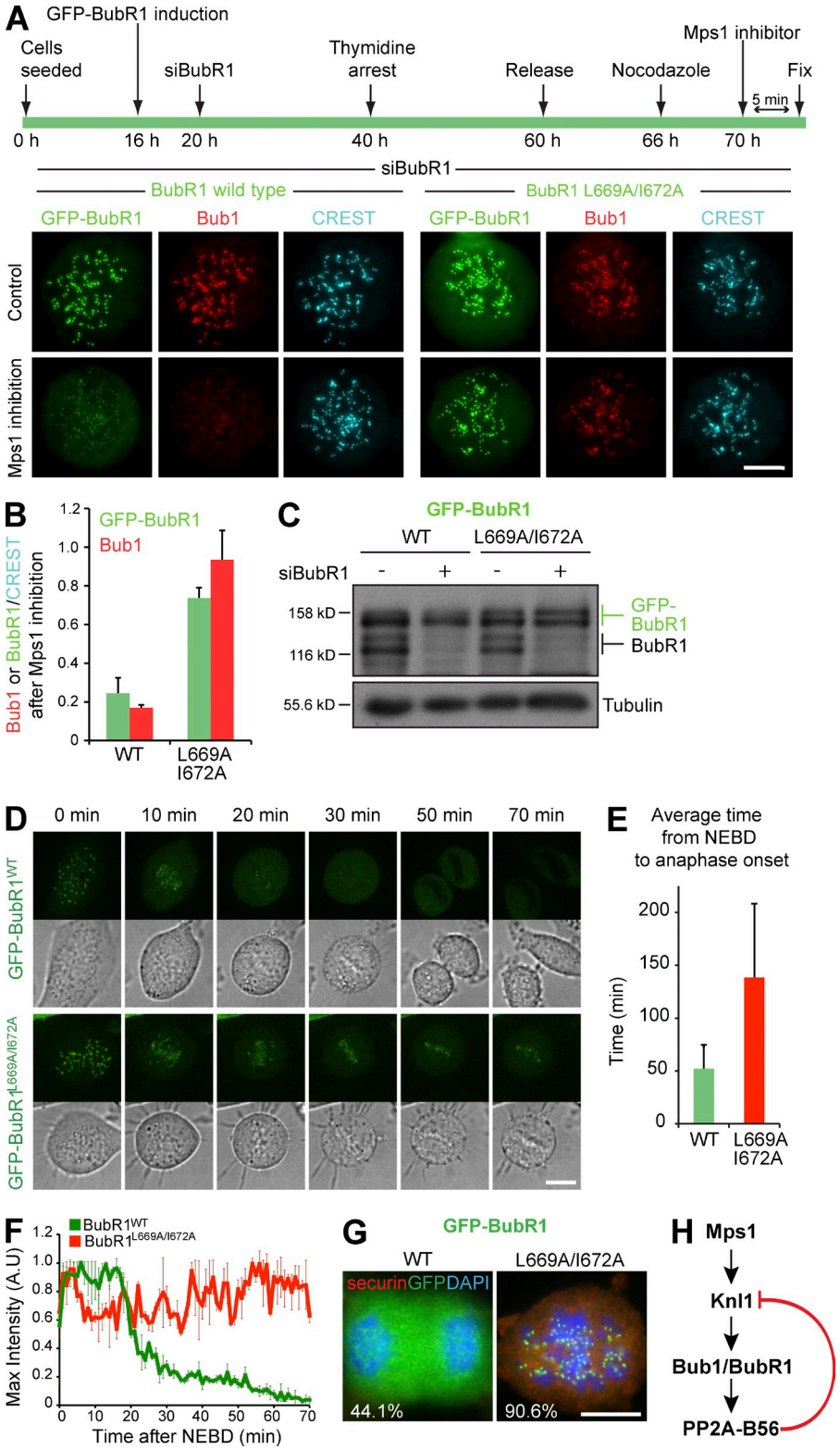

Figure 4. **BubR1-bound PP2A-B56 is required to release BubR1 from the kinetochore upon Mps1 inhibition.** (A) HeLa Flp-in cells expressing GFP-BubR1^{WT} or GFP-BubR1$^{L669A/I672A}$ were treated as indicated in the timeline, fixed, and stained for Bub1 and kinetochores (CREST). Bar, 10 µm. (B) Quantitation of the kinetochore signal ratio of GFP-BubR1/CREST and Bub1/CREST (mean ± SD [error bars]; $n \geq 120$ kinetochores per bar). Images are representative of three independent experiments. (C) Lysates of the cells used in A were blotted for BubR1 and tubulin. (D) GFP-BubR1^{WT} or GFP-BubR1$^{L669A/I672A}$ cells depleted of endogenous BubR1 were imaged on a spinning disc confocal microscope. Bar, 10 µm. (E) Quantitation of the time from nuclear envelope breakdown (NEBD) to anaphase onset (n = 8 for GFP-BubR1^{WT}, n = 8 for GFP-BubR1$^{L669A/I672A}$). (F) Quantitation of maximal GFP-BubR1 kinetochore signal in WT and L669A/I672A cells (n = 3 for both). (G) Cells treated as in A were fixed and stained for securin and DNA (DAPI) after 11 h of release from a thymidine block. Bar, 10 µm. (H) The BubR1-associated pool of PP2A-B56 removes the Mps1-dependent phospho sites on Knl1 that bind Bub3, Bub1, and BubR1 itself, thus establishing a negative feedback loop.

period of Mps1 hypersensitivity is created at the beginning of mitosis when Mps1 can phosphorylate Knl1 in the absence of the opposing phosphatase, generating a maximal SAC protein-binding platform that recruits Bub3/Bub1/BubR1 and associated PP2A-B56. Second, by tying PP2A-B56 to BubR1, the system is poised to extinguish the Bub1/BubR1 kinetochore signal as soon as Mps1 activity drops, yet remain potentially reactivatable because the Mps1 opposing phosphatase declines together with Mps1 levels. In the future it will be interesting to determine what proportion of kinetochore-associated BubR1 is used for mitotic checkpoint complex formation and PP2A-B56 recruitment, respectively.

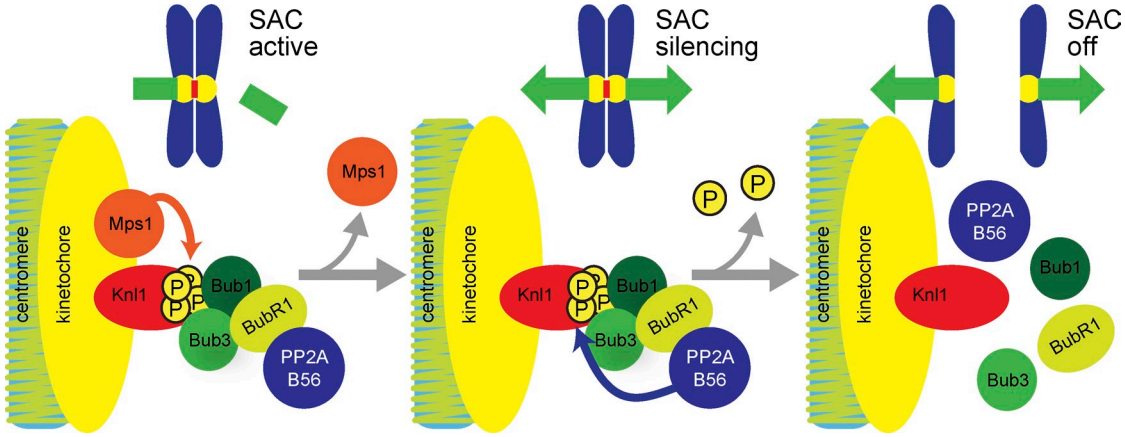

Figure 5. **Model of Knl1 dephosphorylation by BubR1-associated PP2A-B56.** Dephosphorylation of the Mps1 phosphorylation sites on Knl1 by BubR1-associated PP2A-B56 results in removal of the binding sites for Bub1, Bub3, and BubR1 when Mps1 activity drops upon successful microtubule–kinetochore attachment. This leads to loss of Bub1 and BubR1 from the kinetochore and initiation of SAC silencing.

Materials and methods

Reagents and antibodies

General laboratory chemicals were obtained from Sigma-Aldrich and Thermo Fisher Scientific. Commercially available antibodies were used for actin (mouse Mab; Abcam), B55α (mouse; Santa Cruz Biotechnology, Inc.), B56α (for IF mouse mAb, BD; for WB rabbit, Bethyl Laboratories, Inc.), B56γ (mouse mAb E-6; Santa Cruz Biotechnology, Inc.), B56δ (mouse mAb H5D12; EMD Millipore), BubR1 (mouse mAb 3612; EMD Millipore), Bub1 (rabbit; Bethyl Laboratories, Inc.), CenpA (mouse 3-19; Abcam), Hec1 (mouse mAb G3.23; GeneTex), histone H3 phospho-Thr3 (rabbit; EMD Millipore), His-tag (mouse anti–RGS-His; QIAGEN), Knl1 (rabbit; Bethyl Laboratories, Inc.), PP2CA/B (mouse mAb; BD), PP2A-A (goat; Santa Cruz Biotechnology, Inc.), PPP4C (rabbit; Bethyl Laboratories, Inc.), PPP5C (rabbit; Bethyl Laboratories, Inc.), PPP6C (rabbit; Bethyl Laboratories, Inc.), Sgo2 (rabbit; Bethyl Laboratories, Inc.), and tubulin (mouse mAb DM1A; Sigma-Aldrich). Human CREST serum was obtained from Antibodies Inc. Antibodies to Knl1 phosphorylated at T875 were raised in sheep (Scottish Blood Transfusion Services) and affinity purified using the peptide sequence C+NDMDI(pT)KSYTI (Yamagishi et al., 2012). Affinity purified sheep anti-GFP and anti-GST antibodies were a gift of F. Barr (University of Oxford, Oxford, England, UK). Secondary donkey antibodies against mouse, rabbit, or sheep and labeled with Alexa Fluor 488, Alexa Fluor 555, Alexa Fluor 647, Cy5, or HRP were purchased from Molecular Probes and Jackson ImmunoResearch Laboratories, Inc., respectively. Kinase, phosphatase, and proteasome inhibitors were obtained from Tocris Bioscience and dissolved in DMSO (Mps1 inhibitor AZ3146 20 mM 10,000× stock, PP1/PP2A inhibitor calyculin 10 µM 4,000× stock, proteasome inhibitor MG132 20 mM 1,000× stock, haspin inhibitor 5-iodotubercidine 5 mM 500× stock, nocodazole 0.2 mg/ml 2,000× stock).

Molecular biology

Human PP2A-B56γ, PP2A-B55α, Mis12, BubR1, and Mps1 were amplified from human testis cDNA (Marathon cDNA; Takara Bio Inc.) using Pfu polymerase (Promega). A fragment (aa 728–1,200) of human Knl1 was amplified from ORFeome clone 100069116 (Thermo Fisher Scientific). Mammalian expression constructs for BubR1, PP2A-B56γ, and PP2A-B55α were made using pcDNA5/FRT/TO vectors (Invitrogen) modified to encode the FLAG or EGFP reading frames. For the generation of HeLa cells stably expressing GFP-Mis12 or mCherry-histone H2B and EGFP–α-tubulin, Mis12 was cloned into pEGFP-C2 (Takara Bio Inc.), and histone H2B and α-tubulin were cloned into pCDNA3-based vectors encoding the appropriate tags, the chicken β-actin promoter in the case of α-tubulin to reduce expression, and blasticidin and puromycin selection markers. For the generation of GST-tagged Knl1$^{728\text{-}1200}$, this fragment of Knl1 was cloned into pGEX-5X-1 (GE Healthcare). Recombinant baculoviruses carrying hexahistidine-tagged full-length wt or kinase-dead Mps1 cloned into the pACSG2 vector (BD) were produced using the BaculoGold system (BD). Mutagenesis was performed using the QuikChange method (Agilent Technologies). DNA primers were obtained from Invitrogen. siRNA single duplexes or On-target SMARTPools were obtained from GE Healthcare (see Table S1 for sequences of phosphatase catalytic subunit SMARTPools). PP2A-B55 regulatory subunits were depleted simultaneously by mixing the individual SMARTPools for PPP2R2A, -B, -C, and -D. PP2A-B56 regulatory subunits were depleted simultaneously by mixing single siRNA duplexes targeting each individual regulatory subunit (Foley et al., 2011). The siRNA oligo target sequence for the 3′ UTR of BubR1 was 5′-GCAATCAAGTCTCACAGAT-3′.

Cell culture

HeLa cells were cultured in DMEM containing 10% [vol/vol] bovine calf serum at 37°C and 5% CO_2. For plasmid transfection and siRNA transfection, Mirus LT1 (Mirus Bio LLC) and Oligofectamine (Invitrogen), respectively, were used. Stable HeLa cell lines with single copies of the desired transgene were created using the T-Rex doxycycline-inducible Flp-In system (Invitrogen; Tighe et al., 2004). HeLa cells stably expressing GFP-Mis12 or HeLa cells stably expressing mCherry-histone H2B and EGFP–α-tubulin (Zeng et al., 2010) were generated using a standard transfection protocol and selection with 0.7 mg/ml geneticin or 1.0 µg/ml puromycin and 2.0 µg/ml blasticidin. For synchronization, cells were treated for 20 h with 2.5 mM thymidine, washed three times in PBS and twice with growth medium, and then incubated in fresh growth medium for the indicated time. Sf9 insect cells for the expression of Mps1 wt and kinase-dead (KD) kinase were grown at 27°C and atmospheric CO_2 in TC100 containing 10% [vol/vol] bovine calf serum and 1% [vol/vol] GlutaMAX (Invitrogen).

Protein expression and purification

For the purification of recombinant hexahistidine-tagged full-length wild-type and kinase-inactive D664A Mps1 from Sf9 insect cells, 20 × 10^7 insect cells per construct were infected with the respective viruses at a multiplicity of infection of 10. After 60 h of infection, the cells were collected, washed in cold PBS, and lysed for 10 min in IMAC20 buffer (20 mM Tris-Cl, pH 8.0, 200 mM NaCl, and 20 mM imidazole) containing 0.1% Triton X-100 and a protease inhibitor cocktail (Sigma-Aldrich). The cell lysate was cleared for 30 min at 100,000 *g* at 4°C using an Optima-Max-XP ultracentrifuge (Beckman Coulter) and a TLA-100.3 rotor, after which the cleared lysate was incubated with Ni-NTA beads (QIAGEN). After a 2-h incubation in the cold, the beads were washed extensively with IMAC20, and bound proteins were eluted with IMAC200 (20 mM Tris-Cl, pH 8.0, 200 mM NaCl, and 200 mM imidazole). The peak fractions as judged by SDS-PAGE were pooled and dialyzed against PBS.

GST-tagged Knl1$^{728\text{-}1200}$ was expressed in *Escherichia coli* Bl21 cells. The pellet of a 2 liter bacterial culture was resuspended in 150 mM Hepes, pH 8.0, 300 mM NaCl, 0.5 mM EDTA, 1 mM DTT, and protease inhibitor cocktail (Sigma-Aldrich), and lysed using a homogenizer (Emulsiflex). The lysate was cleared by centrifugation and incubated with glutathione-Sepharose (GE Healthcare) for 2 h in the cold. After extensive washing with lysis buffer, bound proteins were eluted with 100 mM Tris-Cl, pH 8.0, 150 mM NaCl, and 20 mM reduced glutathione. Peak fractions as judged by SDS-PAGE were pooled and dialyzed against 150 mM Hepes, pH 8.0, and 150 mM NaCl.

PP2A-B55 and PP2A-B56 complexes were purified from FLAG-PP2A-B55α– and FLAG-PP2A-B56γ–transfected HEK-293T cells as described previously (Cundell et al., 2013). In brief, three 15-cm dishes of HEK-293T cells per construct (pCDNA5-FLAG-PPP2R2A, pCDNA5-FLAG-PPP2R5C, and empty FLAG vector) were transfected with 8 µg DNA and LT1 transfections reagent (Mirus Bio LLC) according to the manufacturer's instructions. After 40 h of transfection, the cells were pelleted, washed in cold PBS, and lysed for 15 min on ice in 20 mM Tris-Cl, pH 8.0, 150 mM NaCl, 1% [vol/vol] Triton X-100, and 1× protease inhibitor cocktail. The lysates were cleared by centrifugation in an Eppendorf centrifuge (14,000 rpm, 4°C, 15 min), and the cleared lysates were incubated with FLAG-agarose beads (Sigma-Aldrich) for 3 h in the cold. The beads were washed twice with lysis buffer, four times with 20 mM Tris-Cl, pH 8.0, 150 mM NaCl, and 0.1% [vol/vol] Triton X-100; once with 20 mM Tris-Cl, pH 8.0, and 150 mM NaCl; and once with 100 mM Tris-Cl, pH 8.0, and 1 mM $MnCl_2$. PP2A complexes were eluted twice with 50 µl of elution buffer (0.2 mg/ml FLAG peptide in 20 mM Tris-Cl, pH 8.0, 150 mM NaCl, and 1 mM $MnCl_2$), each, in a Vibrax rocker at room temperature. Beads and eluates were separated by centrifugation, DTT and glycerol were added to 1 mM and 20% final concentration, respectively, and the eluted proteins were snap frozen in liquid nitrogen.

Immunofluorescence analysis

Immunofluorescence analysis was performed as described previously (Dunsch et al., 2011) using PTEMF buffer (20 mM Pipes-KOH, pH 6.8, 0.2% Triton X-100, 1 mM $MgCl_2$, 10 mM EGTA, and 4% formaldehyde) for fixation. Antibody dilutions were performed in PBS, 2% [wt/vol] BSA, and 0.1% [vol/vol] Triton X-100, except for phospho-Knl1 antibodies that were diluted in PBS, 2% [wt/vol] BSA, and 0.3% [vol/vol] Triton X-100. Samples on 1.5-thickness coverslips were imaged using a 60× 1.35 NA oil immersion objective lens on a microscope system (BX61; Olympus) equipped with filter sets for DAPI, EGFP/Alexa Fluor 488, Alexa Fluor 555, and Alexa Fluor 647 (Chroma Technology Corp.); a CoolSNAP HQ2 camera (Roper Scientific); and MetaMorph 7.5 imaging software (GE Healthcare). Image z stacks comprising 12 images 0.2 µm apart were collected and maximum projected to give a single image for each color channel. The different color channels were then combined in MetaMorph to give a 24-bit RGB image. These were cropped in Photoshop CS3 and imported into Illustrator CS3 (both from Adobe) for figure production. Quantitations of kinetochore intensities were performed using Volocity (PerkinElmer) or ImageJ software. Background-corrected kinetochore intensities (3–4 cells; ≥40 kinetochores per cell) determined by placing a 7 × 7-pixel circular region of interest over individual kinetochores were normalized to CREST or CenpA signal as indicated. Analysis of kinetochore intensities was performed in Excel (Microsoft). All immunofluorescence experiments shown are representatives of at least three independent experiments.

Spindle checkpoint silencing assay

For SAC silencing assays, HeLa cells were seeded into 6-well dishes with coverslips and treated with siRNA to phosphatase subunits (Thermo Fisher Scientific) for 48 h. See Table S1 for siRNA sequences. Nocodazole (0.1 µg/ml = 0.33 µM) was then added for an additional 12–14 h. Subsequently, cells were treated with MG132 (20 µM) alone or with a mixture of MG132 and Mps1 inhibitor AZ3146 (2 µM) for 5 min at 37°C. Cells were fixed using PTEMF solution (Dunsch et al., 2011) and stained with the indicated antibodies. Human CREST antiserum or CenpA antibody were used for kinetochore control staining.

Phosphatase assays

Recombinant GST-Knl1$^{728\text{-}1200}$ was phosphorylated with recombinant Mps1 for 30 min at 30°C in 50 mM Tris-Cl, pH 7.3, 50 mM KCl, 10 mM $MgCl_2$, 20 mM sodium β-glycerophosphate, 15 mM EGTA, 0.1 mM ATP, 1 mM DTT, and 1 µCi [^{32}P]γ-ATP per reaction. Mps1 kinase activity was then inhibited with 2 µM AZ3146 (MPS1 inhibitor; Hewitt et al., 2010), and different amounts of purified phosphatase complex were added. Dephosphorylation was assessed by loss of phospho-specific pKnl1-pT875 signal.

For dephosphorylation of GFP-Mis12 complexes, GFP-Mis12 was immunoprecipitated from 3 × 10^7 nocodazole-arrested GFP-Mis12 HeLa cells lysed in mitotic lysis buffer (100 mM Tris-Cl, pH 7.5, 150 mM NaCl, 1% IGEPAL, 2,500 U/ml benzonase [Sigma-Aldrich], and 1× protease and phosphatase inhibitor mix [Sigma-Aldrich]). The immunoprecipitate was washed into dephosphorylation buffer (100 mM Tris-Cl, pH 7.4, 100 mM KCl, 20 mM $MgCl_2$, 40 mM sodium β-glycerophosphate, 30 mM EGTA, and 2 µm AZ3146) and evenly aliquoted into three tubes. PP2A-B55 or PP2A-B56 complexes containing equivalent amounts of catalytic subunit were added, an input sample was immediately withdrawn from each reaction, and the beads were incubated for 30 min at 30°C. Beads and supernatants were separated by centrifugation, and the beads were washed three times with reaction buffer before addition of Laemmli buffer.

Live cell microscopy

Live cell imaging was performed using a spinning disc confocal system (Ultraview Vox; PerkinElmer) mounted on an inverted microscope (IX81; Olympus) equipped with an EM charge-coupled device camera (C9100-13; Hamamatsu Photonics) and controlled by Volocity software. Cells were plated in 35-mm dishes with a 14-mm diameter 1.5-thickness coverglass window in the bottom (MatTek Corporation) and placed in a 37°C and 5% CO_2 environmental chamber (Tokai Hit) on the microscope stage. Imaging was performed using a 60× NA 1.4 oil immersion objective lens, 4% laser power for 488 and 561 lasers, and 30–100 ms exposure time. Typically, 19 planes, 0.6 µm apart were imaged every minute. Maximum intensity projections of the fluorescent channels for image analysis were performed using Volocity to create 24-bit RGB TIF files. For figure production, images were cropped in ImageJ and placed into Illustrator CS3 (Adobe). For analysis of GFP-BubR1 kinetochore signal, background-corrected maximum GFP-BubR1 intensities per cell were plotted. Data analysis was performed using Prism 6 (GraphPad) or Excel software.

Online supplemental material

Fig. S1 contains additional control experiments for the SAC phosphatase siRNA screen. Fig. S2 shows the effects of depleting single PP2A-B56 subunits on SAC silencing assays and live cell imaging of cells in the absence of all PP2A-B56 subunits. Fig. S3 contains additional control immunofluorescence stainings for the pKnl1-pT875 antibody, Knl1 and pKnl1-pT875 blots of GFP-Mis12 IP dephosphorylations, and the demonstration that depletion of Sgo2 does not affect the loss of BubR1 from kinetochores when Mps1 is inhibited. Table S1 gives siRNA target sequences. Online supplemental material is available at http://www.jcb.org/cgi/content/full/jcb.201406109/DC1.

We thank Lukas Hutter and Drs. Daniel Hayward, Francis Barr, and Béla Novák for critical reading of the manuscript and insightful discussions. We are particularly grateful to Dr. Francis Barr for help with figure preparation. We thank Dr. Kang Zeng for generating the GFP-Mis12 stable cells. We thank Drs. G. Kops and A. Saurin for communicating unpublished results.

Research in U. Gruneberg's laboratory is supported by a Medical Research Council Senior Non-Clinical Research fellowship (MR/K006703/1). This work was initiated while U. Gruneberg held a Cancer Research UK Career Development fellowship (C24085/A8296). R.N. Bastos is supported by a Cancer Research UK program grant award (C20079/A15940) to Francis A. Barr, and D. Mangat is supported by an EP Abraham Research Fund studentship. Live cell imaging was performed at the Micron Oxford Advanced Bioimaging Unit (Wellcome Trust Strategic Award 091911).

The authors declare no competing financial interests.

Submitted: 25 June 2014
Accepted: 21 August 2014

References

Barr, F.A., P.R. Elliott, and U. Gruneberg. 2011. Protein phosphatases and the regulation of mitosis. *J. Cell Sci.* 124:2323–2334. http://dx.doi.org/10.1242/jcs.087106

Bollen, M., D.W. Gerlich, and B. Lesage. 2009. Mitotic phosphatases: from entry guards to exit guides. *Trends Cell Biol.* 19:531–541. http://dx.doi.org/10.1016/j.tcb.2009.06.005

Cundell, M.J., R.N. Bastos, T. Zhang, J. Holder, U. Gruneberg, B. Novak, and F.A. Barr. 2013. The BEG (PP2A-B55/ENSA/Greatwall) pathway ensures cytokinesis follows chromosome separation. *Mol. Cell.* 52:393–405. http://dx.doi.org/10.1016/j.molcel.2013.09.005

De Antoni, A., S. Maffini, S. Knapp, A. Musacchio, and S. Santaguida. 2012. A small-molecule inhibitor of Haspin alters the kinetochore functions of Aurora B. *J. Cell Biol.* 199:269–284. http://dx.doi.org/10.1083/jcb.201205119

Dunsch, A.K., E. Linnane, F.A. Barr, and U. Gruneberg. 2011. The astrin-kinastrin/SKAP complex localizes to microtubule plus ends and facilitates chromosome alignment. *J. Cell Biol.* 192:959–968. http://dx.doi.org/10.1083/jcb.201008023

Espeut, J., D.K. Cheerambathur, L. Krenning, K. Oegema, and A. Desai. 2012. Microtubule binding by KNL-1 contributes to spindle checkpoint silencing at the kinetochore. *J. Cell Biol.* 196:469–482. http://dx.doi.org/10.1083/jcb.201111107

Foley, E.A., and T.M. Kapoor. 2013. Microtubule attachment and spindle assembly checkpoint signalling at the kinetochore. *Nat. Rev. Mol. Cell Biol.* 14:25–37. http://dx.doi.org/10.1038/nrm3494

Foley, E.A., M. Maldonado, and T.M. Kapoor. 2011. Formation of stable attachments between kinetochores and microtubules depends on the B56-PP2A phosphatase. *Nat. Cell Biol.* 13:1265–1271. http://dx.doi.org/10.1038/ncb2327

Funabiki, H., and D.J. Wynne. 2013. Making an effective switch at the kinetochore by phosphorylation and dephosphorylation. *Chromosoma*. 122:135–158. http://dx.doi.org/10.1007/s00412-013-0401-5

Hewitt, L., A. Tighe, S. Santaguida, A.M. White, C.D. Jones, A. Musacchio, S. Green, and S.S. Taylor. 2010. Sustained Mps1 activity is required in mitosis to recruit O-Mad2 to the Mad1-C-Mad2 core complex. *J. Cell Biol.* 190:25–34. http://dx.doi.org/10.1083/jcb.201002133

Jelluma, N., T.B. Dansen, T. Sliedrecht, N.P. Kwiatkowski, and G.J. Kops. 2010. Release of Mps1 from kinetochores is crucial for timely anaphase onset. *J. Cell Biol.* 191:281–290. http://dx.doi.org/10.1083/jcb.201003038

Kitajima, T.S., T. Sakuno, K. Ishiguro, S. Iemura, T. Natsume, S.A. Kawashima, and Y. Watanabe. 2006. Shugoshin collaborates with protein phosphatase 2A to protect cohesin. *Nature*. 441:46–52. http://dx.doi.org/10.1038/nature04663

Kiyomitsu, T., C. Obuse, and M. Yanagida. 2007. Human Blinkin/AF15q14 is required for chromosome alignment and the mitotic checkpoint through direct interaction with Bub1 and BubR1. *Dev. Cell*. 13:663–676. http://dx.doi.org/10.1016/j.devcel.2007.09.005

Krenn, V., A. Wehenkel, X. Li, S. Santaguida, and A. Musacchio. 2012. Structural analysis reveals features of the spindle checkpoint kinase Bub1-kinetochore subunit Knl1 interaction. *J. Cell Biol.* 196:451–467. http://dx.doi.org/10.1083/jcb.201110013

Krenn, V., K. Overlack, I. Primorac, S. van Gerwen, and A. Musacchio. 2014. KI motifs of human Knl1 enhance assembly of comprehensive spindle checkpoint complexes around MELT repeats. *Curr. Biol.* 24:29–39. http://dx.doi.org/10.1016/j.cub.2013.11.046

Kruse, T., G. Zhang, M.S. Larsen, T. Lischetti, W. Streicher, T. Kragh Nielsen, S.P. Bjørn, and J. Nilsson. 2013. Direct binding between BubR1 and B56-PP2A phosphatase complexes regulate mitotic progression. *J. Cell Sci.* 126:1086–1092. http://dx.doi.org/10.1242/jcs.122481

Liu, D., M. Vleugel, C.B. Backer, T. Hori, T. Fukagawa, I.M. Cheeseman, and M.A. Lampson. 2010. Regulated targeting of protein phosphatase 1 to the outer kinetochore by KNL1 opposes Aurora B kinase. *J. Cell Biol.* 188:809–820. http://dx.doi.org/10.1083/jcb.201001006

London, N., S. Ceto, J.A. Ranish, and S. Biggins. 2012. Phosphoregulation of Spc105 by Mps1 and PP1 regulates Bub1 localization to kinetochores. *Curr. Biol.* 22:900–906. http://dx.doi.org/10.1016/j.cub.2012.03.052

Maciejowski, J., K.A. George, M.E. Terret, C. Zhang, K.M. Shokat, and P.V. Jallepalli. 2010. Mps1 directs the assembly of Cdc20 inhibitory complexes during interphase and mitosis to control M phase timing and spindle checkpoint signaling. *J. Cell Biol.* 190:89–100. http://dx.doi.org/10.1083/jcb.201001050

Meadows, J.C., L.A. Shepperd, V. Vanoosthuyse, T.C. Lancaster, A.M. Sochaj, G.J. Buttrick, K.G. Hardwick, and J.B. Millar. 2011. Spindle checkpoint silencing requires association of PP1 to both Spc7 and kinesin-8 motors. *Dev. Cell*. 20:739–750. http://dx.doi.org/10.1016/j.devcel.2011.05.008

Pinsky, B.A., C.R. Nelson, and S. Biggins. 2009. Protein phosphatase 1 regulates exit from the spindle checkpoint in budding yeast. *Curr. Biol.* 19:1182–1187. http://dx.doi.org/10.1016/j.cub.2009.06.043

Primorac, I., J.R. Weir, E. Chiroli, F. Gross, I. Hoffmann, S. van Gerwen, A. Ciliberto, and A. Musacchio. 2013. Bub3 reads phosphorylated MELT repeats to promote spindle assembly checkpoint signaling. *eLife*. 2:e01030. http://dx.doi.org/10.7554/eLife.01030

Qian, J., B. Lesage, M. Beullens, A. Van Eynde, and M. Bollen. 2011. PP1/Repo-man dephosphorylates mitotic histone H3 at T3 and regulates chromosomal aurora B targeting. *Curr. Biol.* 21:766–773. http://dx.doi.org/10.1016/j.cub.2011.03.047

Rosenberg, J.S., F.R. Cross, and H. Funabiki. 2011. KNL1/Spc105 recruits PP1 to silence the spindle assembly checkpoint. *Curr. Biol.* 21:942–947. http://dx.doi.org/10.1016/j.cub.2011.04.011

Schittenhelm, R.B., R. Chaleckis, and C.F. Lehner. 2009. Intrakinetochore localization and essential functional domains of *Drosophila* Spc105. *EMBO J.* 28:2374–2386. http://dx.doi.org/10.1038/emboj.2009.188

Shepperd, L.A., J.C. Meadows, A.M. Sochaj, T.C. Lancaster, J. Zou, G.J. Buttrick, J. Rappsilber, K.G. Hardwick, and J.B. Millar. 2012. Phosphodependent recruitment of Bub1 and Bub3 to Spc7/KNL1 by Mph1 kinase maintains the spindle checkpoint. *Curr. Biol.* 22:891–899. http://dx.doi.org/10.1016/j.cub.2012.03.051

Sliedrecht, T., C. Zhang, K.M. Shokat, and G.J. Kops. 2010. Chemical genetic inhibition of Mps1 in stable human cell lines reveals novel aspects of Mps1 function in mitosis. *PLoS ONE*. 5:e10251. http://dx.doi.org/10.1371/journal.pone.0010251

Suijkerbuijk, S.J., M. Vleugel, A. Teixeira, and G.J. Kops. 2012. Integration of kinase and phosphatase activities by BUBR1 ensures formation of stable kinetochore-microtubule attachments. *Dev. Cell*. 23:745–755. http://dx.doi.org/10.1016/j.devcel.2012.09.005

Tanno, Y., T.S. Kitajima, T. Honda, Y. Ando, K. Ishiguro, and Y. Watanabe. 2010. Phosphorylation of mammalian Sgo2 by Aurora B recruits PP2A and MCAK to centromeres. *Genes Dev.* 24:2169–2179. http://dx.doi.org/10.1101/gad.1945310

Tighe, A., V.L. Johnson, and S.S. Taylor. 2004. Truncating APC mutations have dominant effects on proliferation, spindle checkpoint control, survival and chromosome stability. *J. Cell Sci.* 117:6339–6353. http://dx.doi.org/10.1242/jcs.01556

Vanoosthuyse, V., and K.G. Hardwick. 2009. A novel protein phosphatase 1-dependent spindle checkpoint silencing mechanism. *Curr. Biol.* 19:1176–1181. http://dx.doi.org/10.1016/j.cub.2009.05.060

Vleugel, M., E. Tromer, M. Omerzu, V. Groenewold, W. Nijenhuis, B. Snel, and G.J. Kops. 2013. Arrayed BUB recruitment modules in the kinetochore scaffold KNL1 promote accurate chromosome segregation. *J. Cell Biol.* 203:943–955. http://dx.doi.org/10.1083/jcb.201307016

Welburn, J.P., M. Vleugel, D. Liu, J.R. Yates III, M.A. Lampson, T. Fukagawa, and I.M. Cheeseman. 2010. Aurora B phosphorylates spatially distinct targets to differentially regulate the kinetochore-microtubule interface. *Mol. Cell*. 38:383–392. http://dx.doi.org/10.1016/j.molcel.2010.02.034

Xu, Y., Y. Chen, P. Zhang, P.D. Jeffrey, and Y. Shi. 2008. Structure of a protein phosphatase 2A holoenzyme: insights into B55-mediated Tau dephosphorylation. *Mol. Cell*. 31:873–885. http://dx.doi.org/10.1016/j.molcel.2008.08.006

Xu, Z., B. Cetin, M. Anger, U.S. Cho, W. Helmhart, K. Nasmyth, and W. Xu. 2009. Structure and function of the PP2A-shugoshin interaction. *Mol. Cell*. 35:426–441. http://dx.doi.org/10.1016/j.molcel.2009.06.031

Xu, P., E.A. Raetz, M. Kitagawa, D.M. Virshup, and S.H. Lee. 2013. BUBR1 recruits PP2A via the B56 family of targeting subunits to promote chromosome congression. *Biol. Open*. 2:479–486. http://dx.doi.org/10.1242/bio.20134051

Yamagishi, Y., C.H. Yang, Y. Tanno, and Y. Watanabe. 2012. MPS1/Mph1 phosphorylates the kinetochore protein KNL1/Spc7 to recruit SAC components. *Nat. Cell Biol.* 14:746–752. http://dx.doi.org/10.1038/ncb2515

Zeng, K., R.N. Bastos, F.A. Barr, and U. Gruneberg. 2010. Protein phosphatase 6 regulates mitotic spindle formation by controlling the T-loop phosphorylation state of Aurora A bound to its activator TPX2. *J. Cell Biol.* 191:1315–1332. http://dx.doi.org/10.1083/jcb.201008106

Zhang, G., T. Lischetti, and J. Nilsson. 2014. A minimal number of MELT repeats supports all functions of KNL1 in chromosome segregation. *J. Cell Sci.* 127:871–884. http://dx.doi.org/10.1242/jcs.139725